Monthly Notices
of the
ROYAL ASTRONOMICAL SOCIETY

Mon. Not. R. Astron. Soc. **415,** 3693–3705 (2011) doi:10.1111/j.1365-2966.2011.18985.x

Observational evidence of dissipative photospheres in gamma-ray bursts

Felix Ryde,[1,2⋆] Asaf Pe'er,[3] Tanja Nymark,[1,2] Magnus Axelsson,[1,2] Elena Moretti,[1,2] Christoffer Lundman,[1,2] Milan Battelino,[1,2] Elisabetta Bissaldi,[4] James Chiang,[5] Miranda S. Jackson,[1,2] Stefan Larsson,[6] Francesco Longo,[7,8] Sinead McGlynn[1,9] and Nicola Omodei[5]

[1]*Department of Physics, Royal Institute of Technology (KTH), AlbaNova, SE-106 91 Stockholm, Sweden*
[2]*The Oskar Klein Centre for Cosmoparticle Physics, AlbaNova, SE-106 91 Stockholm, Sweden*
[3]*Harvard–Smithsonian Center for Astrophysics, Cambridge, MA 02138, USA*
[4]*Institut für Astro- und Teilchenphysik and Institut für Theoretische Physik, Leopold-Franzens-Universität Innsbruck, A-6020 Innsbruck, Austria*
[5]*Department of Physics and SLAC National Accelerator Laboratory, W. W. Hansen Experimental Physics Laboratory, Kavli Institute for Particle Astrophysics and Cosmology, Stanford University, Stanford, CA 94305, USA*
[6]*Department of Astronomy, Stockholm University, SE-106 91 Stockholm, Sweden*
[7]*Istituto Nazionale di Fisica Nucleare, Sezione di Trieste, I-34127 Trieste, Italy*
[8]*Dipartimento di Fisica, Università di Trieste, I-34127 Trieste, Italy*
[9]*Exzellenzcluster Universe, Technische Universität München, D-85748 Garching, Germany*

Accepted 2011 April 29. Received 2011 April 8; in original form 2011 March 3

ABSTRACT

The emission from a gamma-ray burst (GRB) photosphere can give rise to a variety of spectral shapes. The spectrum can retain the shape of a Planck function or it can be broadened and have the shape of a Band function. This fact is best illustrated by studying GRB090902B. The main gamma-ray spectral component is initially close to a Planck function, which can only be explained by emission from the jet photosphere. Later, the same component evolves into a broader Band function. This burst thus provides observational evidence that the photosphere can give rise to a non-thermal spectrum. We show that such a broadening is most naturally explained by subphotospheric dissipation in the jet. The broadening mainly depends on the strength and location of the dissipation, the magnetic field strength and the relation between the energy densities of thermal photons and electrons. We suggest that the evolution in spectral shape observed in GRB090902B is due to a decrease in the bulk Lorentz factor of the flow, leading to the main dissipation becoming subphotospheric. Such a change in the flow parameters can also explain the correlation observed between the peak energy of the spectrum and low-energy power-law slope, α, a correlation commonly observed in GRBs. We conclude that photospheric emission could indeed be a ubiquitous feature during the prompt phase in GRBs and play a decisive role in creating the diverse spectral shapes and spectral evolutions that are observed.

Key words: radiation mechanisms: thermal – gamma-ray burst: general.

1 INTRODUCTION

The original fireball model of gamma-ray bursts (GRBs) predicts a strong photospheric component during the prompt phase (Goodman 1986; Paczyński 1986). The very high optical depth to scattering expected near the base of the flow implies that, regardless of the exact nature of the emission process, the resulting spectrum thermalizes and is observed as a Planck spectrum. However, only a few GRBs have been identified to be dominated by a Planck spectrum (Ryde 2004). Non-thermal spectra are more typically observed (Preece et al. 1998; Kaneko et al. 2006). Moreover, if the photosphere occurs far from where the acceleration of the flow ceases (the saturation radius), the thermal component is weakened by adiabatic expansion. Most of the flow energy is then in the form of kinetic energy and only a thermal relic is left.

It was therefore argued that the dominating emission mechanism should instead be optically thin synchrotron emission (Tavani 1996), emitted by relativistic electrons. These are accelerated following kinetic energy dissipation that takes place above the photosphere. Such dissipation could, for instance, result from internal shocks within the flow (e.g. Rees & Mészáros 1994). However, this

⋆E-mail: fryde@kth.se

paradigm has, in turn, several severe problems. Foremost, in order to reproduce the observed sub-MeV spectral peak by synchrotron emission, a strong magnetic field, typically of the order of $B \sim 10^5$–10^6 G, is required. In such a strong magnetic field, the shocked electron population is expected to cool rapidly, producing a typical spectrum which is in stark contradiction to the observed spectral shape (Crider et al. 1997, Preece et al. 1998; Ghisellini & Celotti 1999; see further discussion in e.g. Ryde et al. 2006).

The challenges for optically thin synchrotron emission led to the revival of the idea that the jet photosphere may play an important role, in one way or another, in the formation of the spectrum (Eichler & Levinson 2000; Mészáros & Rees 2000). Mészáros & Rees (2000) proposed that several spectral components exist in the gamma-ray band, including a Planck spectrum from the photosphere. Such a spectrum can appear as a Band function when it is observed in a narrow energy band. Indeed, Ryde (2005), who studied time-resolved spectra from subpulses, showed that in many cases the GRB spectra in the BATSE energy range (∼25–1900 keV) are statistically indistinguishable between fits with a Band function and with a Planck function combined with a power law (BB+pl). In many cases the BB+pl model is even preferred over the Band function. In addition, the thermal component was found, in these fits, to have a recurring behaviour during individual pulses: the temperature decay is well fitted by a characteristic broken power law (PL) in time (see Ryde & Pe'er 2009 for further details). Even though the BATSE observations were limited by the narrow energy band, they thus gave an indication that a photospheric emission does, in fact, exist in many bursts and that GRBs in general have several spectral components in the gamma-ray band.

Moreover, Ryde & Pe'er (2009) argued that GRB spectra should typically be more complicated than a single Band function, when observed over a broader energy range. This is because approximately 10 per cent of all *Compton Gamma-ray Observatory* (*CGRO*) BATSE bursts have, during their entire duration, time-resolved spectra with a Band function high-energy spectral slope $\beta > -2$ (Kaneko et al. 2006). The peak in the energy flux (νF_ν) of these bursts must therefore be above the BATSE energy range, at an energy higher than the determined spectral break. Ryde & Pe'er (2009) also studied the few bursts for which there are simultaneous and time-resolved data available from both BATSE and EGRET-TASC. They found that several breaks indeed exist in the spectrum (see also Barat et al. 1998). While the overall power peak, in the studied bursts, lay in the EGRET range, Ryde & Pe'er (2009) interpreted the break in the BATSE range as a subdominant thermal peak. Recently, similar conclusions were drawn by Guiriec et al. (2011) and Zhang et al. (2011).

There are thus strong arguments, both theoretical and observational, that the photospheric emission plays an important role in the spectral formation during the prompt phase in GRBs. Indeed, recently the *Fermi Gamma-ray Space Telescope* (energy range of 8 keVto > 300 GeV) has observed bursts in which a photospheric component is present and several spectral components are required (Ryde et al. 2010; Guiriec et al. 2011). However, many bursts observed by the *Fermi* instruments do not show such obvious distinction between a Planck function and other spectral components. The spectral peak is more typically described by a more broadly peaked Band component.

This has, in turn, led to increased interest in the suggestion put forward by Rees & Mészáros (2005), who argued that strong dissipation should naturally occur below and close to the photosphere (see Section 3 for further details). This results from oblique shock waves that are formed at the edges of the jet as it propagates through the star. The dissipated energy results in reprocessing of the original Planck spectrum due to e.g. Comptonization by energetic electrons (Pe'er, Mészáros & Rees 2005, 2006; see also Giannios 2006). This alters the Planck spectrum into the observed spectrum. Emission from the photosphere could therefore have a Band-like character, and its shape should depend on the details of the dissipation of the kinetic energy of the flow. Similar scenarios have recently been discussed by several authors, e.g. Beloborodov (2010), Ioka (2010), Lazzati & Begelman (2010), Toma, Wu & Mészáros (2010) and Bromberg, Mikolitzky & Levinson (2011); see further discussions in Ramirez-Ruiz (2005) and Ruffini et al. (2005).

In this paper, we study the particular spectral evolution of GRB090902B. In this burst, the main spectral component, stemming from the photosphere, exhibits a change in spectral characteristics half-way through the prompt phase. At early times, the thermal component resembles a Planck function, while at late times this component broadens significantly. Based on this study, we further discuss the conditions under which photospheric emission is broadened. We argue that this mechanism can be applicable to more typical spectral evolutions, in which the spectra more gradually evolve from being hard to becoming softer. In particular, we argue that it may provide a natural explanation for the observed variety of spectral shapes in GRBs (in particular the width of the spectral peak). In Section 2, the spectral behaviour of GRB090902B is presented and in Section 3 the effects of subphotospheric shocks on GRB spectra are discussed. In Section 4, we use subphotospheric shocks to explain the spectral evolution in GRB090902B. We discuss our results in Section 5, and we conclude in Section 6.

2 SPECTRAL BEHAVIOUR OF GRB090902B

The bright and long burst GRB090902B was detected by the *Fermi Gamma-ray Space Telescope* by its two instruments: the Large Area Telescope (LAT; energy range from 100 MeV to > 300 GeV) and the Gamma-ray Burst Monitor (GBM; 8 keV–40 MeV). The burst lies at a redshift of $z = 1.822$ (Cucchiara et al. 2009). It is one of the strongest bursts detected by the *Fermi* and the emission at energies larger than 8 keV lasted for approximately 25 s. The most energetic photon with an energy of $33.4^{+2.7}_{-3.5}$ GeV was detected at 82 s after the trigger by the LAT. The light curve of the prompt phase is shown in Fig. 1.

During the prompt phase of approximately 25 s, two distinct, separate components are observed throughout the duration: a peaked MeV component (modelled with a Band function) and a PL component. The PL component is clearly detected at energies both below and above the MeV peak (observations are made in the range of 8 keV to ∼30 GeV). Moreover, while the MeV peak undergoes substantial spectral evolution the PL component remains relatively steady with the photon index of approximately −1.9 (Abdo et al. 2009b).

At early times (first 12.5 s; epoch 1) the pronounced MeV peak is so steep and narrow that it must be attributed to emission from the photosphere (e.g. fig. 1 in Ryde et al. 2010; see also Section 2.2). However, during the second half of the prompt phase, which lasted for another 12 s (epoch 2), the MeV peak differs significantly from a Planck function, resembling a typical Band spectrum.[1]

[1] Note that a Planck spectrum can in principle be approximated by a 'Band' function, but with very steep $\alpha = 1$ and $\beta \to -\infty$. We use the term 'Band' to describe spectrum that is not as steep.

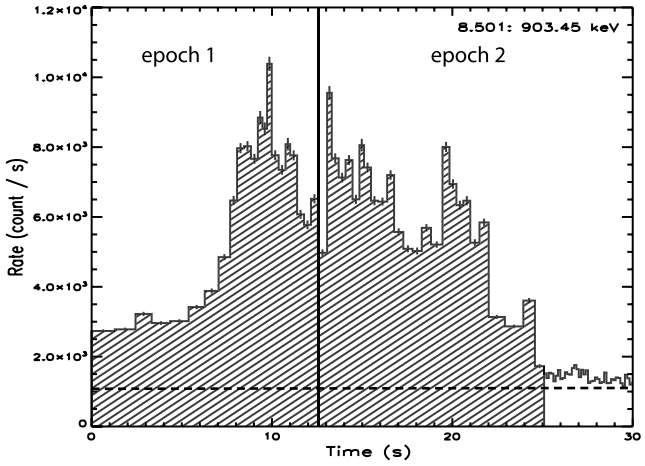

Figure 1. Light curve of GRB090902B, observed by Na I 1 in the energy range 8.5–904 keV. The presented time binning is used in the analysis and the two epochs discussed in the paper are divided by the vertical line. The thin dashed line is the background level.

We argue here that, although the spectral shape of the MeV peak varies, it is most likely that it has the same origin throughout the burst. The reasons are the following. (i) The spectra are clearly separated into two spectral components throughout the burst duration, namely an MeV peak and an independent PL component (Fig. 3). (ii) Although the MeV peak broadens, the PL component remains relatively steady (see Abdo et al. 2009b). (iii) The spectra of the MeV bump during epoch 2 are still inconsistent with the expected non-thermal spectrum; fast-cooling electrons yield $\alpha = -1.5$ (see Section 2.2). (iv) To get a synchrotron peak energy to lie in a similar energy range as the thermal peak during epoch 1 requires an unreasonable coincidence. (v) On the other hand, as we show in Section 4, the broadening of the thermal peak by subphotospheric dissipation easily reproduces the observed spectrum. Therefore, we argue that this burst provides an observational evidence that the emission from a GRB photosphere does not necessarily need to be a narrow, Planck-like spectrum but can be significantly broadened. This burst is the best example available to study the details of the photosphere and its emission.

In general, the spectral evolution in GRBs is more gradual than observed in GRB090902B. The steepest subpeak slopes (largest values of α) are typically found at the very beginning of the prompt phase and only during a small fraction of the burst duration. The spectra thereafter rapidly soften (Crider et al. 1997; Ghirlanda, Celotti & Ghisellini 2003). The particular property of the spectral evolution in GRB090902B is the substantial fraction of the burst duration during which the emission spectrum is Planck-like. This allows the establishment of its photospheric origin.

Here, we further study the time-resolved spectra by following the analysis performed in Ryde et al. (2010). We use the same detectors (Na I 0, 1 and BGO 0, 1 and LAT front and back), and the time binning was determined by requiring a signal-to-noise ratio (S/N) in the strongest illuminated detector to be at least S/N = 45. The data were fitted using RMFIT[2] version 3.0 using the Castor *C*-statistic (*C*-stat) to determine the goodness of fit. The light curve with the time binning used is shown in Fig. 1. Here the burst is divided into two epochs: one comprising data from within 12.5 s of the trigger, referred to as epoch 1 (analysed in Ryde et al. 2010) and another comprising data after 12.5 s until the end of the burst, referred to as epoch 2.

2.1 Band function fits

A model consisting of a Band function (Band et al. 1993) (for the dominating MeV component) and a PL component fits the time-resolved spectra well during epoch 1 (Ryde et al. 2010). This is also the case for our fits. However, inspection of the *C*-stat maps of the parameters reveals that the error ranges are not well constrained in several bins. The reason for this was determined to be the low amplitude of the PL in these bins. In these cases, we froze the PL amplitude to the value found in the fit and then performed a new fit to determine values and uncertainty intervals for the remaining parameters. For all bins, the values of the parameters found before freezing the PL amplitude were consistent with the values found after the amplitude was frozen.

Table 1 shows the results of our fits to the time-resolved spectra indicating α (photon index of the subpeak PL), β (photon index of the super-peak PL), $E_{\rm p}$ (peak energy) and the photon index of the PL component. Fig. 2 shows the evolution of the shape of the MeV component. The upper panels show the parameters α and β over the full duration of the burst (0–25 s). The index of $\alpha = -2/3$ expected from optically thin synchrotron emission is indicated (Rybicki & Lightman 1979) as well as $\alpha = 0$, the spectral slope expected from, e.g. jitter radiation and from extreme cases of inverse Compton emission from a delta function distribution of electrons (Jones 1968). The errors on the data points represent asymmetric, 1σ uncertainties on the parameter values found from the fitting.

In Fig. 2, it is clearly seen that the spectral shape exhibits a change in character at approximately 12.5 s after the trigger, as noted already by Ryde et al. (2010). From being very peaked, with $\alpha \sim 0.3$ and $\beta \sim -3.5$ and with a spectral width of the peak[3] $w = 6$, the spectrum broadens significantly. During the second epoch, the typical values of $\alpha \sim -0.6$ and $\beta \sim -2.5$. As a result, the spectral width has increased between the first and second epochs by more than a factor of 2, to typically $w = 10$–20. In the lower right-hand panel in Fig. 2, the best-fitting Band function of the MeV peak is plotted for two instants: at 6.5 and 22 s after the GBM trigger. These spectra have been aligned to each other's $E_{\rm p}$ values in order to highlight the spectral broadening: while the typical spectrum at epoch 1 is close to a Planck function, the spectrum at epoch 2 has a shape that is typical for a GRB spectrum, that is, a Band function.

Even though the change in the spectral character between the epochs is clear from the above discussion, there are still important similarities between the epochs. Most notably, Abdo et al. (2009b) clearly showed that the PL component remains relatively steady during the spectral evolution of the prompt phase. Moreover, during the time period 15–17 s, the MeV component becomes relatively hard again. The similarities between these spectra and the epoch 1 spectra are shown in Fig. 3. Here a spectrum from epoch 1 (8.1–8.5 s) and a spectrum from epoch 2 (15.9–16.4 s) are shown. The broadening of the MeV component, compared to the epoch 1 spectra, is still apparent, even though the broadening

[2] R. S. Mallozzi, R. D. Preece & M. S. Briggs, 'RMFIT, a light curve and spectral analysis tool', © Robert D. Preece, University of Alabama in Huntsville.

[3] We here define the spectral width, w, as the ratio $E_{\rm high}/E_{\rm low}$, where energy fluxes $F_{\rm E}(E_{\rm low})$ and $F_{\rm E}(E_{\rm high})$ are equal to half the peak flux ($F_{\rm peak}/2$) below and beyond the peak, respectively.

Table 1. Results of spectral fits to the data of GRB090902B during the time 12.54–24.58 s after the burst trigger (epoch 2). Uncertainties marked unc indicate that the parameter is unconstrained. Results for epoch 1 are presented in Ryde et al. (2010).

Time (s)	PL index	$E_{\rm peak}$	α	β	C-stat/d.o.f.
12.54–13.06	$-2.04^{+0.09}_{-0.07}$	113^{+13}_{-10}	$-0.53^{+0.36}_{-0.28}$	$-2.37^{+0.10}_{-0.13}$	589.69/598
13.06–13.31	$-1.65^{+0.12}_{-0.51}$	268^{+21}_{-21}	$-0.54^{+0.08}_{-0.07}$	$-2.63^{+0.16}_{-0.22}$	548.28/598
13.31–13.70	$-1.97^{+0.16}_{-0.13}$	259^{+22}_{-24}	$-0.73^{+0.15}_{-0.10}$	$-2.58^{+0.16}_{-0.23}$	524.54/598
13.70–14.08	$-1.78^{+0.08}_{-0.09}$	482^{+24}_{-26}	$-0.73^{+0.05}_{-0.04}$	$-3.93^{+0.71}_{-17.6}$	517.21/598
14.08–14.46	$-2.88^{+0.43}_{-0.83}$	611^{+44}_{-33}	$-0.50^{+0.09}_{-0.10}$	$-2.81^{+0.12}_{-0.15}$	551.20/597
14.46–14.85	$-2.46^{+0.04}_{-0.04}$	599^{+41}_{-37}	$-0.50^{+0.08}_{-0.07}$	$-2.76^{+0.12}_{-0.15}$	585.00/598
14.85–15.10	$-3.87^{+2.82}_{-0.98}$	603^{+48}_{-40}	$-0.57^{+0.07}_{-0.07}$	$-2.67^{+0.11}_{-0.13}$	445.00/598
15.10–15.49	$-3.12^{+0.04}_{-0.04}$	674^{+29}_{-28}	$-0.32^{+0.05}_{-0.05}$	$-2.83^{+0.10}_{-0.11}$	617.42/598
15.49–15.87	$-1.94^{+0.04}_{-0.03}$	720^{+41}_{-38}	$-0.29^{+0.08}_{-0.08}$	$-2.81^{+0.12}_{-0.12}$	584.36/598
15.87–16.38	$-1.99^{+0.06}_{-0.73}$	435^{+30}_{-31}	$-0.22^{+0.13}_{-0.12}$	$-2.67^{+0.22}_{-0.21}$	559.96/597
16.38–16.77	$-1.88^{+0.05}_{-0.05}$	540^{+33}_{-26}	$-0.21^{+0.10}_{-0.10}$	$-3.59^{+0.46}_{\rm unc}$	608.65/597
16.77–17.28	$-1.88^{+0.05}_{-0.06}$	326^{+30}_{-25}	$-0.27^{+0.17}_{-0.16}$	$-2.63^{+0.17}_{-0.26}$	613.26/597
17.28–17.79	$-1.99^{+0.11}_{-1.21}$	400^{+34}_{-31}	$-0.48^{+0.13}_{-0.12}$	$-2.67^{+0.20}_{-0.35}$	539.27/597
17.79–18.30	$-5.90^{+1.41}_{-2.08}$	236^{+24}_{-16}	$-0.62^{+0.09}_{-0.10}$	$-2.19^{+0.04}_{-0.02}$	574.43/597
18.30–18.82	$-5.40^{\rm unc}_{\rm unc}$	425^{+37}_{-20}	$-0.87^{+0.06}_{-0.05}$	$-2.35^{+0.04}_{-0.06}$	536.23/597
18.82–19.46	$-1.38^{+0.09}_{-0.16}$	352^{+26}_{-34}	$-0.84^{+0.06}_{-0.05}$	$-2.47^{+1.59}_{-0.10}$	723.50/598
19.46–19.84	$-1.34^{+0.09}_{-0.12}$	358^{+22}_{-23}	$-0.62^{+0.06}_{-0.05}$	$-2.89^{+0.23}_{-0.36}$	539.89/598
19.84–20.22	$-1.41^{+0.09}_{-0.12}$	521^{+35}_{-33}	$-0.86^{+0.04}_{-0.04}$	$-2.99^{+0.26}_{-0.45}$	488.24/598
20.22–20.61	$-4.22^{+0.71}_{-0.16}$	328^{+26}_{-28}	$-0.83^{+0.07}_{-0.12}$	$-2.71^{+0.96}_{-0.20}$	691.51/598
20.61–20.99	$-1.96^{+0.27}_{-0.31}$	280^{+23}_{-27}	$-0.70^{+0.11}_{-0.06}$	$-2.53^{+0.13}_{-0.16}$	531.45/598
20.99–21.50	$-2.07^{\rm unc}_{\rm unc}$	234^{+15}_{-22}	$-0.85^{+0.11}_{-0.05}$	$-2.56^{+1.17}_{-0.17}$	736.42/598
21.50–22.02	$-1.70^{+0.12}_{-0.29}$	275^{+18}_{-25}	$-0.74^{+0.07}_{-0.05}$	$-2.51^{+0.17}_{-0.12}$	756.01/598
22.02–22.91	$-2.15^{+0.81}_{\rm unc}$	174^{+41}_{-53}	$-1.25^{+0.31}_{-0.05}$	$-2.06^{+0.06}_{-0.07}$	639.88/598
22.91–23.94	$-1.39^{+0.07}_{-0.10}$	448^{+160}_{-107}	$-1.50^{+0.05}_{-0.05}$	$-2.36^{+0.17}_{-0.17}$	807.17/598
23.94–24.58	$-2.13^{+0.27}_{-0.12}$	197^{+33}_{-27}	$-0.82^{+0.25}_{-0.20}$	$-2.22^{+0.08}_{-0.10}$	546.56/598

is not as large as for the other epoch 2 spectra. These observations are thus strong indications of that the emission during the two epochs are of similar origin, i.e. a photospheric and an optically thin component.

Fig. 4 shows the $E_{\rm p}$ evolution as a function of time. The averaged value of $E_{\rm p}$ is lower during epoch 2 compared to epoch 1.

In spite of the variations in the spectrum of the MeV component, it dominates the spectral energy flux throughout the burst duration. The ratio of the energy flux in the MeV peak relative to the total *Fermi* gamma-ray flux (MeV peak + PL component) is in the range of 80–95 per cent during the entire burst duration. This mainly results from a decrease in the amplitude of the PL component towards the end.

2.2 Significance of the hard α values

During epoch 1 the averaged value of α is $\langle\alpha\rangle = 0.11$, and for several of the time bins the value of α is even steeper, with $\alpha \gtrsim 0.2$. These very hard spectra are particularly challenging for non-thermal models. Synchrotron and inverse Compton emission in the fast-cooling regime are expected to produce a spectral slope of $\alpha = -1.5$. Here, we consider the most extreme scenario with $\alpha = 0$ (Jones 1968; Epstein & Petrosian 1973). We therefore want to estimate the significance of rejecting $\alpha = 0$ for these spectra. This allows us to determine the significance of the conclusion that neither synchrotron nor inverse Compton scattering processes can explain the spectra.

This is done by simulating spectra with RMFIT v3.0 using the set of observed spectral parameter values of the Band function fit. We use the *Fermi* detector responses for GRB090902B and take into account the Poissonian nature of the observed counts and realistic background emission. The simulated count distributions are then fitted in the same way as the real data. The parameter values we find can then be studied.

We illustrate the procedure on the seventh time bin (6.3–7.0 s) which has the hardest observed value of $\alpha = 0.3 \pm 0.1$ (Ryde et al. 2010). We start with the null hypothesis that the spectrum observed in this time bin has an actual value $\alpha = 0$. We therefore freeze α at this value, and, based on the best-fitting parameters we find from the data, we perform 100 000 simulations. This large number of simulations allows us to make a proper estimation of the significance level. The simulated spectra are then fitted with the Band function with all parameters free to vary. The distribution of the values of α that we find is shown in Fig. 5. The distribution is approximately Gaussian and is slightly skewed. It has a mean value of $\alpha = 0.01$ and a standard deviation of 0.068. The inset in Fig. 5 is a magnification of the distribution around $\alpha = 0.3$. This figure shows that eight out of the 100 000 simulated spectra have fits with values of α

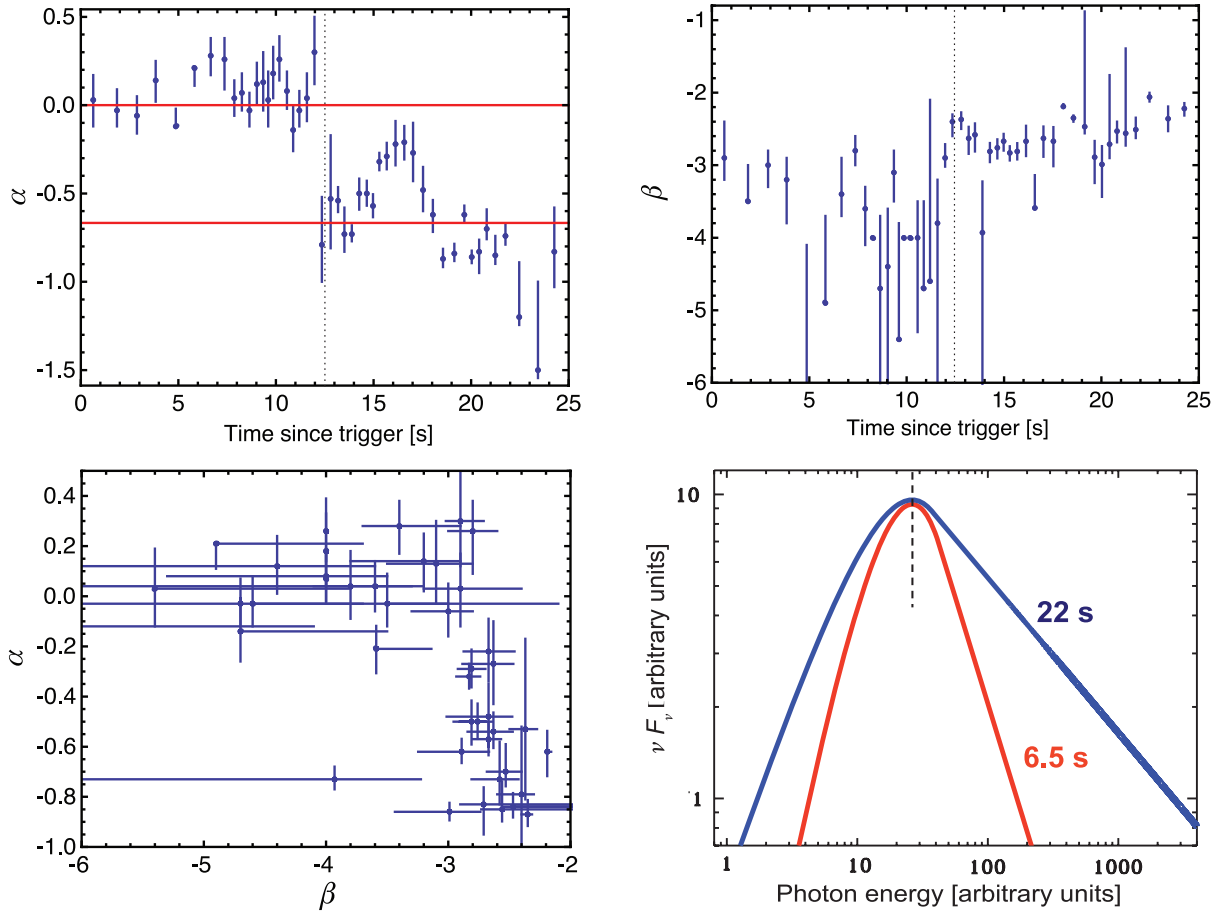

Figure 2. Evolution of the MeV component in GRB090902B. Upper left-hand panel: evolution of low-energy photon index α. Two horizontal lines are shown, which correspond to $\alpha = 0$, the most extreme value expected for inverse Compton models and $\alpha = -2/3$, expected for optically thin synchrotron emission for a slow cooling electron population. The dashed line indicates 12.5 s. Upper right-hand panel: evolution of the high-energy PL index β. Lower left-hand panel: correlation between α and β. Note that some points have only one-sided error bars indicating that they are unconstrained in the other direction. Lower right panel: peak-aligned Band functions corresponding to the fits at two different times, illustrating the spectral broadening. These two times include the narrowest and the broadest Band spectra.

greater than 0.3. This gives the probability that a spectrum with an actual value $\alpha = 0$ should be observed with $\alpha > 0.3$ by chance to be 8×10^{-5}. Therefore, the null hypothesis can be rejected on a very high confidence level for this bin. Most of the measured values of α during epoch 1 are, though, not significantly inconsistent with $\alpha = 0$ (see Fig. 2). In any case, the epoch 1 spectra are challenging for purely non-thermal emission models, since $\alpha = 0$ is only expected under somewhat extreme conditions; see Section 5.1 for further details. The expected value is rather $\alpha = -1.5$, which is produced by a population of fast-cooling electrons (Ghisellini & Celotti, 1999).

The averaged value of α during epoch 2 is $\langle\alpha\rangle = -0.65$. This value is still significantly inconsistent with $\alpha = -1.5$. For instance, the 42nd time bin (19.84–20.22 s) has one of the softest values of α with $\alpha = -0.86 \pm 0.04$. Even though, when we perform a fit with α frozen at -1.5 to this time bin, we find an increase of the C-stat value from 488 to 1167 for 597 degrees of freedom. The hypothesis of having $\alpha = -1.5$ can therefore be rejected on a significant level of less than 10^{-10}. We also point at the fact that several of the fitted spectra in epoch 2 have $\alpha \sim -0.2$; the 32nd time bin (15.87–16.38 s) has the hardest spectrum with $\alpha = -0.2 \pm 0.1$, approaching the values of α from epoch 1, see Fig. 2.

3 SUBPHOTOSPHERIC HEATING AND ITS EFFECT ON THE EMISSION SPECTRUM

As we saw above, GRB090902B is a particularly interesting burst since initially the main spectral component is close to a Planck function but later evolves into a broader Band function. Indeed, as we will see in this section, the emitted spectrum that is expected from a GRB photosphere depends on the existence of significant dissipation close to the photosphere.

3.1 Photospheres and dissipation radius

At small radii the jet outflow in a GRB is opaque due to photons scattering off electrons that are associated with the baryons. As the particle densities decrease the flow eventually becomes transparent, that is, the optical depth to scattering falls below unity. Such a baryonic photosphere is expected to be at (e.g. Mészáros et al. 2002)

$$r_{\rm ph} \sim 4.8 \times 10^{11} \frac{L}{10^{53}\,{\rm erg\,s^{-1}}} \left(\frac{\Gamma}{630}\right)^{-3}\ {\rm cm}, \qquad (1)$$

where the typical value for GRB090902B is used: $L = 10^{53}$ erg s^{-} (Abdo et al. 2009b). We also use the *time-averaged* value for

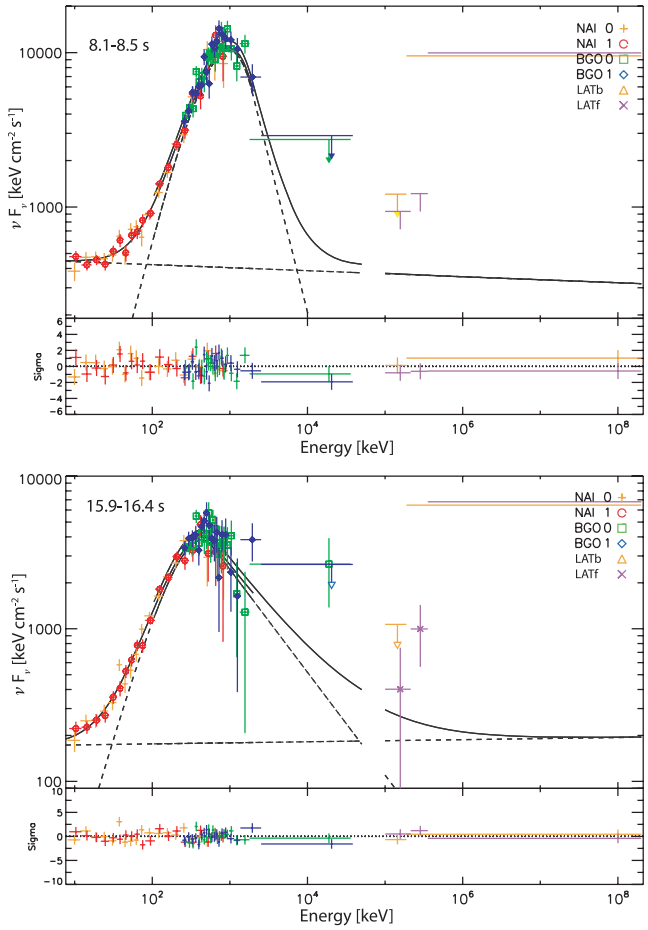

Figure 3. Time-resolved νF_ν spectrum for two time intervals $t = 8.1$–8.5 s (epoch 1) and $t = 15.9$–16.4 s (epoch 2). The Band + PL model is fitted to the data over the GBM + LAT energy ranges. The symbols refer to the different instruments on the *Fermi Gamma-ray Space Telescope*. While there still are similarities between the spectra, the broadening of the MeV component is apparent (compare fig. 1 in Ryde et al. 2010).

$\Gamma = 600\,Y^{1/4} \sim 630$ (Ryde et al. 2010).[4] Here Y denotes the ratio between the total fireball energy and the energy emitted in gamma-rays and can be estimated from afterglow measurements. Cenko et al. (2010) estimated the value to be $Y \sim 1.2$ in the case of GRB090902B.

Pair formation can be significant and modify the spectrum (e.g. Eichler & Levinson 2000; Pe'er & Waxman 2004). Subphotospheric dissipation can lead to copious production of pairs, resulting in a second, pair photosphere above the baryonic photosphere (Mészáros et al. 2002). During the dissipation process, electrons are expected to be accelerated to high energies, thereby emitting energetic photons at energies above the threshold for pair production, $m_e c^2$. These photons then produce pairs by annihilating with the lower energy photons. The created pairs have modest Lorentz factors, $\gamma_e \sim$ few (in the comoving frame). For subphotospheric dissipation these pairs are expected to be more numerous than the baryon-related electrons, and a pair photosphere is expected to be established at

[4] Later we also use the notation $\Gamma_{2.8} \equiv (\Gamma/630)$ and $L_{53} \equiv (L/10^{53}\,\mathrm{erg\,s^{-1}})$. Note that Pe'er et al. (2010) used $\Gamma \sim 1000$ which was estimated for a single time bin used in their analysis.

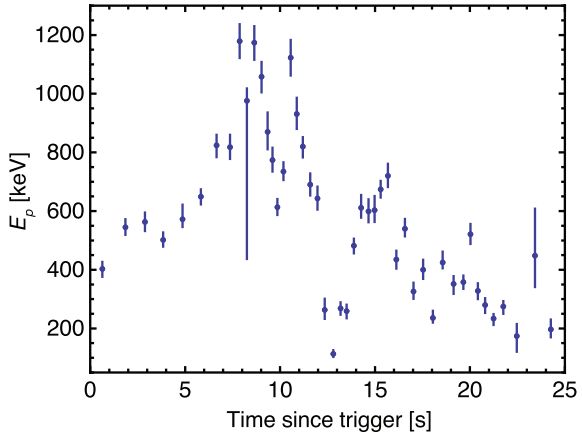

Figure 4. The evolution of the peak energy of the Band function fits, E_p, as a function of time since the GBM trigger.

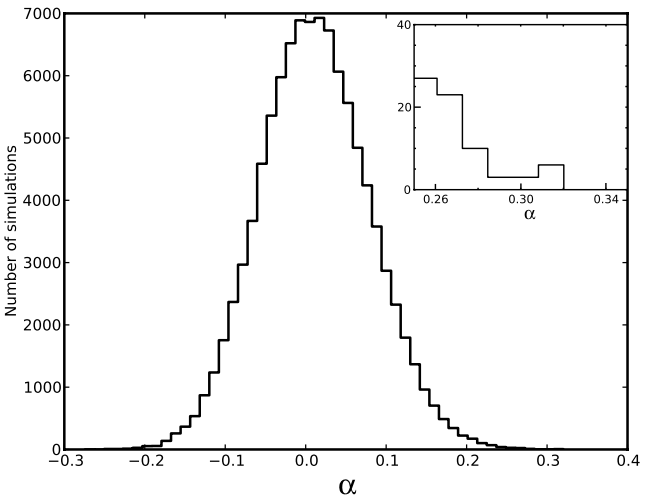

Figure 5. Histogram distribution of α values found from 100 000 simulated spectra. The inlay is a magnification of an interval around $\alpha = 0.3$. See the text for details.

radius (Pe'er & Waxman 2004)

$$r_\pm \sim 8.0 \times 10^{14} \left(\frac{L}{10^{53}\,\mathrm{erg\,s^{-1}}}\right) \epsilon_\pm\, \tilde{\alpha}^{-1} \left(\frac{\Gamma}{630}\right)^{-3} \mathrm{cm}, \qquad (2)$$

where $\epsilon_\pm$ is the fraction of the total fireball energy that is dissipated into photons with comoving energy larger than $m_e c^2$ and is available for pair formation. We define $r_0 = \tilde{\alpha} r_g$ as the effective radius at which the outflow starts to accelerate (in the absence of dissipation): $\tilde{\alpha} \gtrsim 1$ and $r_g \equiv 2GM/c^2 = 3 \times 10^6 (M/10\,\mathrm{M}_\odot)$ cm is the Schwarzschild radius of the central black hole of mass $M = 10\,\mathrm{M}_\odot$. The pair photosphere is above the baryonic photosphere if $\epsilon_\pm > m_e/m_\mathrm{p} = 5.45 \times 10^{-4}$ (Rees & Mészáros 2005).

The existence of a dissipation process is in fact required by the data. Since we see non-thermal spectra in GRBs, this implies that there is a mechanism that dissipates some fraction of the jet kinetic energy. The exact nature of this dissipation is debatable. Several models exist in the literature. The leading ones are as follows: (i) internal shocks in which shells with varying Lorentz factors interact with each other (Rees & Mészáros 1994); (ii) oblique shocks within the funnel in the star (e.g. Morsony et al. 2010); (iii) collisional

dissipation in the flow (Beloborodov 2003); or (iv) in the case of Poynting-flux-dominated flows, the dissipation could result from magnetic reconnection (e.g. Thompson 1994; Giannios & Spruit 2005). The shocked region subsequently cools by emitting photons through, for instance, synchrotron emission and/or inverse Compton emission.

In the internal shocks scenario, dissipative heating is typically assumed to occur well above the photosphere: with variations in the Lorentz factor in the flow of the size $\Delta\Gamma \sim \Gamma$ the internal shocks occur at $r_{\rm sh} \sim 2r_0\Gamma^2 \sim 2.1 \times 10^{13}$ cm. However, Rees & Mészáros (2005) pointed out that due to the jet edge effects oblique shocks might form below and close to the photosphere:

$$r_{\rm sh} \sim 2r_0\Gamma^2\theta_j \sim 6.3 \times 10^{11}\ \tilde{\alpha} \left(\frac{\Gamma}{630}\right)^2 \frac{\theta_j}{3\times10^{-2}}{\rm cm}, \quad (3)$$

where θ_j is the nozzle opening half-angle.

It thus follows that internal shocks may naturally be expected in proximity of the photosphere. While the details of these process are still highly uncertain, this problem is extensively being studied numerically. Indeed, numerical simulations of a jet penetrating though the core of the progenitor show that such shocks do indeed occur (Lazzati, Morsony & Begelman 2009; Mizuta, Nagataki & Aoi 2011; Nagakura et al. 2011). We note that similar conclusions are drawn for other dissipation processes as well (Giannios & Spruit 2005; Giannios 2006; Giannios & Spruit 2007; Tchekhovskoy, McKinney & Narayan 2008; Beloborodov 2010). For example, McKinney & Uzdensky (2010) show that in highly magnetized jets most of the dissipation due to magnetic reconnection mechanisms should indeed occur close to the photosphere.

3.2 Broadening of the Planck spectrum: analytical arguments

The energy that is dissipated in subphotospheric shocks partly thermalizes again to an extent that depends on the conditions at the dissipation site, particularly on the optical depth. Detailed calculations of the thermalization process of such shocks by Pe'er et al. (2006), and in Section 3.3, show that a large variety of spectral shapes can be achieved. Similar results are found in magnetic reconnection models (e.g. Giannios 2006). In particular, Pe'er et al. (2006) showed that the Planck function that is injected into the dissipation region is modified to a varying extent depending on the dissipation fractions and the optical depth. The Planck spectrum therefore loses its original shape and the outgoing photospheric emission has a non-thermal shape. The resulting spectrum can have a rather complex spectral shape. As we show here, under plausible conditions in many cases it can be described as a smoothly broken PL.

While detailed numerical results are presented below, we give here some basic analytical arguments to describe the conditions under which significant modification of the spectrum can take place.

Assume that the dissipation process, regardless of its exact nature, produces a population of energetic electrons with characteristic Lorentz factor $\gamma_{\rm e} \gg 1$. These electrons cool by Compton scattering the thermal (photospheric) photons on a time-scale given by $t_{\rm cool} \simeq m_{\rm e}c/(4/3)\gamma_{\rm e}\sigma_{\rm T}u_{\rm ph}$. Here, $u_{\rm ph}$ is the energy density in the thermal photon component, and $\sigma_{\rm T}$ is Thomson cross-section. This loss time can be compared to the dynamical time of the problem, $t_{\rm dyn} = r/\Gamma c$ to obtain (see Pe'er et al. 2005)

$$\frac{t_{\rm loss}}{t_{\rm dyn}} = \frac{3}{4}\frac{m_{\rm e}c^2\Gamma}{\gamma_{\rm e}\sigma_{\rm T}u_{\rm ph}r} = \frac{3}{4}\frac{u_{\rm el}}{\gamma_{\rm e}^2 u_{\rm ph}\tau_{\gamma{\rm e}}}. \quad (4)$$

Here, r is the dissipation radius, $\tau_{\gamma{\rm e}} = (r/\Gamma)n_{\rm e}\sigma_{\rm T}$ is the optical depth to photon scattering by the electrons and $u_{\rm el} = \gamma_{\rm e}n_{\rm e}m_{\rm e}c^2$ is the energy density in the electron component. Thus, for steady outflow luminosity and Lorentz factor, there is a one to one correspondence between the dissipation radius and the optical depth, $r \propto \tau_{\gamma{\rm e}}$. For subphotospheric dissipation, as is considered here, $\tau_{\gamma{\rm e}} > 1$. Thus, for $u_{\rm el} \lesssim u_{\rm ph}$, the ratio in equation (4) is less than unity, regardless of the value of $\gamma_{\rm e}$. While the value of $\gamma_{\rm e}$ is not well constrained theoretically, most acceleration models predict $\gamma_{\rm e} \gtrsim 100$, which automatically implies a low ratio[5] in equation (4). Thus, we can conclude that regardless of the exact nature of the dissipation process, the electrons are expected to cool rapidly on a time-scale much shorter than the dynamical time. This is provided that (i) the dissipation occurs below or not too high above the photosphere and (ii) that the energy that is being dissipated is not much larger than the energy density in the photosphere. The rapid cooling is due to Comptonization of the thermal component; obviously, synchrotron emission further contributes to the rapid cooling of the electrons.

This rapid cooling implies that the electrons lose most of the energy imparted to them by the dissipation process. This energy is used to upscatter the photospheric photons, as well as to emit synchrotron photons. Part of this energy is converted into pairs by upscattered photons that are energetic enough.

The distribution of the rapidly cooled electrons reaches a quasi-steady state: when the electrons are cold enough, inverse Compton scattering becomes inefficient, while other processes, such as direct Compton heating or synchrotron self-absorption, heat the (cold) electrons. The electron distribution can therefore be approximated as a (quasi-)Maxwellian distribution, with characteristic temperature $T_{\rm e}$. As long as the dissipative process that heats the electrons (or introduces a population of energetic electrons into the plasma) exists, the steady temperature of the electrons is inevitably higher than the temperature of the photospheric (thermal) photons: $T_{\rm e} \gtrsim T_\gamma$.

The plasma is therefore characterized by two temperatures, T_γ and $T_{\rm e}$. Due to the rapid cooling, during most of the dynamical time the scatterings take place between the thermal photons and the cold electrons. Since $T_{\rm e} \gtrsim T_\gamma$, the thermal photons gain energy, resulting in modification of the Wien part of the Planck spectrum, to produce a smoother cut-off at high energies (above the thermal peak). The exact shape of the spectrum at these energies (which corresponds to 'β' in Band fits) depends on the optical depth and the ratio of the energy densities in the electrons and photon components. A significant shift can be obtained if the Compton (or equivalently Kompaneet's) y parameter is of the order of a few (which translates to the optical depth of a few), and energy densities in the electron and photon components are roughly comparable.

Interestingly, somewhat similar conditions are required in order to obtain a significant modification to the Rayleigh–Jeans part of the Planck spectrum. This part is modified if two conditions are met: first, a significant number of photons at energies below the thermal peak must be introduced into the plasma. The most natural way to obtain a large density of cold photons is via synchrotron radiation. This emission is expected at low energies, resulting from emission

[5] At the saturation radius, which is the inner-most radius at which dissipation can occur, the energy density in the photon field $u_{\rm ph}$ is comparable to the kinetic energy density. As the dissipation converts an unknown fraction (<100 per cent) of the kinetic energy to the electrons, if the photospheric radius is not much above the saturation radius, the assumption $u_{\rm el} \lesssim u_{\rm ph}$ holds.

from the cold electrons. In order to obtain a significant flux, a strong magnetic field is thus needed. The second condition is that upscattering of these photons should lead to energies comparable to the original thermal photons. The condition here is again $y \geq 1$, which, due to the low value of T_e is translated into $\tau_{\gamma e} \gtrsim$ few.

We further note that if the optical depth $\tau_{\gamma e} \to \infty$, the spectrum approaches either a Planck or Wien spectrum, as the energy given to the electrons is distributed among the electrons and the photons. If the energy given to the electrons by the dissipation process is much larger than the energy in the thermal component, $u_{el} \gg u_{ph}$, then the non-thermal part of the spectrum is significantly more luminous than the thermal part. In such a scenario, the thermal part may not be detectable (for very high optical depth, the resulting Planck or Wien spectrum will have a temperature that is different than the original temperature of the photosphere).

We thus conclude that the broadening of the Planck spectrum naturally occurs if the following conditions are met: (i) dissipation processes take place below the photosphere, at optical depth of $\tau_{\gamma e} \sim$ few; (ii) the energy given to the electrons is comparable to the energy in the thermal photons component and (iii) a strong magnetic field exists, of the order of $u_B/u_{th} \approx 10$ per cent. See further discussions in Pe'er et al. (2005, 2006), Giannios (2006) and Beloborodov (2010).

3.3 Broadening of the Planck spectrum: detailed numerical simulations

The arguments given in Section 3.2 provide a guideline to possible conditions that can lead to the broadening of the thermal spectrum. However, quantitative results can only be obtained numerically. This is because of the non-linearity of the problem. First, a large number of pairs can in principle be produced. Thus, a rapid electromagnetic cascade may be presented. Secondly, as most of the scatterings occur with cold electrons, the cross-section is Klein–Nishina suppressed, and hence simple analytical approximations to the resulting spectra are absent. Finally, photons and electrons can participate in a large number of processes, such as synchrotron, synchrotron self-absorption and Compton scattering, which can have similar importance.

In order to obtain numerical results, we use the code developed by Pe'er & Waxman (2005) for the study of GRB prompt emission. This code was further modified to the study of photospheric emission by Pe'er et al. (2005, 2006). The numerical code solves self-consistently the kinetic equations that describe a large number of physical processes (synchrotron emission, synchrotron self-absorption, direct and inverse Compton scattering, pair production and annihilation and the development of an electromagnetic cascade) that can take place following the injection of energetic particles close to the photosphere. Its unique integrator enables it to follow the evolution of the particle distribution and spectra over many orders of magnitude in time and hence in energy scales. Thus, it is ideal for studying processes that can take place in regions of high optical depth, in which the characteristic time-scale for interactions is much shorter than the dynamical time. A full description of the code appears in Pe'er & Waxman (2005).

In the scenario considered in our calculations, the exact nature of the dissipation process is not specified. We assume that the outflow is characterized by the steady luminosity L_0 and the constant Lorentz factor Γ. The dissipation is assumed to take place at radius r_i and dissipate some fraction ϵ_d of the kinetic energy. A fraction ϵ_e of this energy is used to accelerate electrons while a fraction ϵ_B is channelled into magnetic fields.

The thermal component is considered as a constant source of thermal photons, which irradiate the interaction region during the whole calculation and interact with the accelerated electrons. After the energy has been dissipated, the evolution of the electron/positron populations and the photon population is followed during one dynamical time, $t_{dyn} = r_i/\Gamma c$, subject to synchrotron radiation, Compton scattering and pair production and annihilation, as well as the constant influx of thermal photons. At the end of the dynamical time all the radiation is assumed to be released, and the emerging spectrum is given by the photon distribution at that time. Since $\tau \gtrsim 1$ at the dissipation site, one should take into account adiabatic expansion until the photons are released at $\tau \sim 1$. However, since the optical depth is not more than a few, adiabatic expansion only marginally affects the spectrum and can be neglected for our purposes (see Pe'er & Waxman 2004 for further details).

The code allows us to quantitatively confirm the analytical results discussed in Section 3.2. For instance, while Comptonization naturally leads to a harder high-energy PL, we find that the optical depth has to be relatively high for the number of scatterings to be large enough to affect the high-energy slope. On the other hand, even larger values of τ lead instead to a steepening of β due to thermalization. Moreover, the slopes of the low-energy PL index, α, depends most strongly (for a individual dissipation scenario) on the strength of the magnetic field generated, i.e. on ϵ_B, giving rise to synchrotron emission. A larger ϵ_B leads to a softer value of α. However, the effect of Comptonization and optical depth counteracts this softening. Therefore, the broadest photospheric spectra are obtained for a strong dissipation occurring at moderate optical depths, typically $\tau \sim 10$. A more detailed accounting of the effects of subphotospheric heating on the photospheric spectrum, using this code, is given in Nymark et al. (in preparation).

If shocks occur above the baryonic photosphere ($\tau \ll 1$), we find that the original Planck function will only be marginally affected by the shocked electrons due to the low number of scatterings that will occur.

Note that in these calculations we consider only one dissipation episode. In reality, several dissipations are expected, making the emerging spectrum a superposition of the spectra from several dissipation episodes (see e.g. Giannios 2008; Pe'er et al. 2011). However, for the purposes of this study, the spectrum resulting from one dissipation episode is sufficient to get an indication of the effects that dissipation can have.

4 APPLICATION TO THE SPECTRAL EVOLUTION IN GRB 090902B

4.1 Epoch 1

In the data analysis above (Section 2.1), we found that the averaged value of the low-energy slope is harder than $\alpha = 0$ during epoch 1 in GRB090902B. Apart from being a constraint on the radiation process, this observation sets constraints on any dissipation process that can have had an influence on the spectral shape, such as constraints on the dissipation fractions of the kinetic energy and dissipation radius.

It is worth noting here, though, that when observing a GRB photosphere we actually expect to observe a superposition of spectra with different temperatures as measured in the observer frame, due to geometrical effects (Pe'er 2008). The result is a slightly broadened spectrum. Therefore the sharpest spectrum is not a Planck function but rather a multicolour blackbody (Pe'er & Ryde 2011; see Lundman et al., in preparation, for further details). This effect

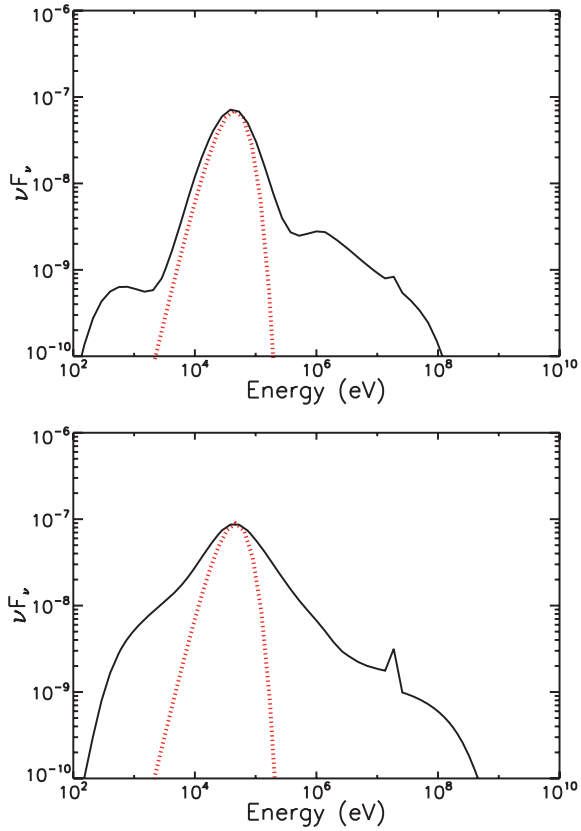

Figure 6. Generic model spectra from subphotospheric shock heating (solid line) illustrating the broadening effect. Upper panel: a low level of energy dissipation only slightly distorts the MeV peak from a Planck function. This spectrum can explain the observed shape at 6.5 s (see Fig. 2). Lower panel: a higher level of energy dissipation broadens the photospheric peak, leading to a Band-like spectrum. This spectrum can explain the spectrum at 22 s (see Fig. 2). The dashed, red line shows the shape of a Planck spectrum at the temperature that corresponds to the peak of the spectrum.

was proposed to explain the deviations from a Planck function that is observed during epoch 1 (Ryde et al. 2010; see also Larsson et al. 2011).

In any case, the simulations of subphotospheric shocks and their effect on the emitted photospheric photon energies, described in Section 3.3, show that dissipation occurring at a low optical depth only marginally affects the emitted photospheric emission. Moreover, in the case of dissipation at moderate optical depths, say $\tau = 10$, a small deviation from a Planck function can only be achieved if the dissipation is relatively weak. Indeed, such dissipation can easily reproduce the observed spectral shapes during epoch 1. As an example we show in the upper panel of Fig. 6 a spectrum found from simulating a shock dissipation in a flow at $\tau = 10$ and with the parameters $\epsilon_{\rm d} = 0.1$, $\epsilon_{\rm e} = 0.1$ and $\epsilon_B = 0.1$. The peak in this spectrum is slightly broader than a Planck function (indicated in the figure with a red dashed line). This shape of the spectrum indeed resembled the MeV peak observed in GRB090902B, e.g. see the red spectrum in the lower right-hand panel of Fig. 2.

Since the observed spectra do not differ much from a Planck spectrum during this epoch, one can thus argue that there cannot have been significant subphotospheric dissipation during this period. Only weak dissipation or no dissipation at all should have occurred. The thermal peak is therefore mainly the original non-processed thermal emission, which was formed at (or close to) the base of the flow, at very high optical depths.

The thermal emission that is observed can either be attributed to a baryonic photosphere or to a pair photosphere. Depending on which photosphere is assumed, a different conclusion will be drawn.

4.1.1 *Baryonic photosphere*

The photospheric radius deduced from the observations to $r_{\rm ph} \sim 10^{12}$ cm can be assumed to be associated to the opacity of the baryonic electrons. This is what is assumed in Ryde et al. (2010) and Pe'er et al. (2010). Furthermore, since the photosphere can be assumed to be non-dissipative, one can use the standard theory discussed in Pe'er et al. (2007) and derive that $r_0 = 10^9\, Y^{-3/2}$ cm $\sim 7.6 \times 10^8$ cm (using the time average values for GRB090902B). The value of r_0 implies an $\tilde{\alpha} \sim 3.3 \times 10^2\, Y^{-3/2} M_1^{-1} \sim 2.5 \times 10^2 M_1^{-1}$, with the notation $M_1 \equiv (M/10\,{\rm M}_\odot)$. According to equation (3), the large value of $\tilde{\alpha}$, and thereby r_0, implies that the dominant fraction of internal shocks occurs well outside of the photosphere, assuming the typical size of the opening angle θ_j. This is consistent with the assumption of a non-dissipative outflow.

4.1.2 *Pair photosphere*

The value of the photospheric radius, $\sim 10^{12}$ cm, that is deduced from the observations can instead be attributed to the pair photosphere. Thus, setting $r_\pm \sim 10^{12}$ cm then equation (2) yields[6] that $\epsilon_\pm\, \tilde{\alpha}^{-1} = 1.25 \times 10^{-3} L_{53}^{-1} \Gamma_{2.8}^3$.

Furthermore, equations (1) and (2) imply that the ratio of the photospheres is $r_\pm / r_{\rm ph} \sim 1.8 \times 10^3\, \epsilon_\pm\, \tilde{\alpha}^{-1}$ in the coasting phase. Thus, $r_\pm / r_{\rm ph} = 2.1\, L_{53}^{-1} \Gamma_{2.8}^3$ and thereby the baryon-photospheric radius is $r_{\rm ph} \sim 5.0 \times 10^{11}\, L_{53} \Gamma_{2.8}^{-3}$ cm. Furthermore, $r_0 = \tilde{\alpha} r_{\rm g} = 2.4 \times 10^9 \epsilon_\pm M_1 L_{53} \Gamma_{2.8}^{-3}$ cm and the saturation radius $r_{\rm s} = \Gamma r_0 = 1.5 \times 10^{12} \epsilon_\pm M_1 L_{53} \Gamma_{2.8}^{-2}$ cm.

Pairs are either created at the base of the flow (Goodman 1986) or in the energy dissipation at the shock. The requirement that $r_{\rm sh} \lesssim r_\pm$ (pairs are created in the shock), with $r_{\rm sh}$ given by equation (3), then corresponds to $\tilde{\alpha} \lesssim 1.6$. From the estimate of $\epsilon_\pm\, \tilde{\alpha}^{-1}$ above this is equivalent of $\epsilon_\pm < 1.58 \times 10^{-3}$. This value implies that in this scenario $r_0 \sim 3 \times 10^6$ cm and $r_{\rm s} \sim 2 \times 10^9$ cm for GRB090902B. This implies that the characteristic initial temperature of the fireball is of the order of $T_0 \sim 4$ MeV (e.g. Rees & Mészáros 2005). Therefore, the expected observed temperature $T = T_0 (r_\pm / r_{\rm s})^{-2/3}$ is approximately 100 keV due to adiabatic expansion. We note that this is a factor of a few below the measured peak energy values. However, the assumption of adiabatic expansion is not necessarily valid since energy dissipation occurs below the photosphere to create the pairs. As discussed in Section 3.1, the heating is most probably continuous due to oblique shocks.

Assuming that the photospheric emission that we are observing is due to the pair photosphere thus results in a value of r_0 which is similar to the generally assumed value for the jet bounding radius. It naturally alleviates the concern that the value, found for the baryonic photosphere ($r_0 \sim 10^8$ cm), is too large. It can thus be argued that it is indeed the pair photosphere we are observing. We note, however, that Zhang, Woosley & Heger (2004) found typical values close to $r_0 \gtrsim 10^8$ cm, since the jet is not well collimated at the centre thus

[6] Using $\Gamma \sim 1000$, which is inferred from opacity arguments (Abdo et al. 2009b), $r_{\rm ph} \sim 2 \times 10^{12}$ cm and $\epsilon_\pm\, \tilde{\alpha}^{-1} \sim 5 \times 10^{-3}$.

preventing the acceleration. This value is similar to what we deduce for the baryonic photosphere.

4.2 Epoch 2

During epoch 2 strong dissipation has to occur at a moderate optical depth, $\tau \sim$ few, in order to broaden the MeV bump. From simulating various dissipation scenarios (described in Section 3.3), we conclude, in particular, that the low-energy slope is mainly determined by the contribution of synchrotron emission (ϵ_B). For instance, a PL distribution of electrons, produced in the dissipation process, is expected to have a peak energy at $\gamma_m \sim \epsilon_e(m_p/m_e) = 1860\epsilon_e$. For the typical parameters for GRB090902B, this translates into a peak of the synchrotron spectrum at $E_m^{\rm synch} = 186\ L_{53}^{1/2}\epsilon_{b,-1}^{1/2}\epsilon_{e,-1}R_{12}^{-1}$ keV, which is less than the average thermal peak lying at $E_p^{\rm thermal} = 2.82\langle kT\rangle \sim 840$ keV. This is still the case if ϵ_b and ϵ_e are somewhat larger, approaching the equipartition values.

The lower panel in Fig. 6 shows an example spectrum from a simulation of a shock dissipation at the same optical depth as before ($\tau = 10$), but with an increased energy dissipation. In this example, the dissipation fractions are given by $\epsilon_d = 0.2$, $\epsilon_e = 0.3$, $\epsilon_B = 0.3$. This spectrum is similar in shape to the blue spectrum in Fig. 2, illustrating that subphotospheric heating indeed can explain the change in the spectral shape that is observed in epoch 2.

4.3 Transition between the two epochs

Variations at the base of the flow are expected to lead to the rapid variation of Γ and $r_{\rm ph}$ of the photosphere, down to a time-scale of $r_0\theta_j/c$ (Rees & Mészáros 2005). This causes varying properties of the dissipation, such as its strength and where it occurs relative to the photosphere.

Due to strong dependence on the Lorentz factor of the ratio $r_{\rm sh}/r_{\rm ph} \propto \Gamma^5$ a change in Γ (apart from variation in the other parameters) can easily alter the dissipation pattern and thereby the appearance of the photospheric spectrum. A decrease in Γ is, for instance, able to cause $r_{\rm ph}$ to become larger than $r_{\rm sh}$, that is, shocks mainly appear below the baryonic photosphere – subphotospheric shocks. Such a change is hence a plausible explanation of the change in the spectrum at ∼12.5 s in GRB090902B. Indeed, in both the baryonic (Section 4.1.1) and pair scenarios (Section 4.1.2) the bulk of the dissipation site then moves from being above $r_{\rm ph}$ to being below it, mainly due to a drop in Γ.

In the photospheric model, the peak of the spectrum (which is measured by E_p) should be closely related to the temperature of the photosphere. This is, for instance, illustrated by Fig. 6. Furthermore, in deriving the Lorentz factor, Γ, from the observables, we note that it most strongly depends on the temperature ($\Gamma \propto T^{1/2}$; Pe'er et al. 2007). The evolutions of Γ and kT are expected to track each other. We therefore argue that variations in E_p are closely related to corresponding variations in Γ (apart from the Doppler boost). In Fig. 4, we show that there is a drop in the averaged E_p between epochs 1 and 2. This thus indicates that a drop occurred in the averaged temperature at this time and thereby also a drop in Γ.

The change in Γ leads to a change in the dissipation pattern, according to the discussion above, and thereby the spectral shape. Indeed, Fig. 7 shows a correlation between E_p and α, reinforcing this interpretation; a decrease in E_p corresponds to a decrease in Γ, which leads to more subphotospheric heating thereby broadening the spectrum (a decrease of α). This is most clearly illustrated by the local increase in E_p observed around 15 s (see Fig. 4), which corresponds to a local increase in α, indicating less subphotospheric heating.

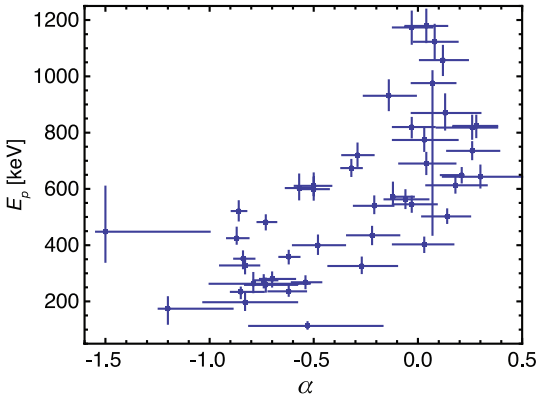

Figure 7. Correlation between E_p and α. Interpreting E_p as related to the temperature of the photosphere; this can be explained by the expected relation between temperature and spectral width in the presence of subphotospheric heating.

5 DISCUSSION

The remarkable property of GRB 090902B is that it is dominated, at early times, by a very peaked spectral component in addition to a PL component. This peaked component, which has a spectral shape very close to a Planck function, can only be explained by emission from the photosphere. As we have seen in the analysis above, at late times the spectrum of this peaked component is broadened into a spectrum that can be described by a Band function with an α slope of approximately −0.6 and a β slope of approximately −2.5. We note that this is close to the spectral shape usually attributed to GRBs (Kaneko et al. 2006). Since there is a continuous change in shape, even though it occurs over a short period compared to the burst duration, it has to be concluded that the photosphere emission continues during the second half of the burst. The consequence of this conclusion is that the photosphere emission spectrum can have a large variety of shapes, which reflect the dissipation processes in the flow. We have argued that this burst provides observational evidence for subphotospheric heating.

This mechanism provides a natural explanation to the observed variety of spectral shapes in GRBs. In addition, the more typical spectral evolution, in which the spectra gradually become softer, can be explained by a gradual change in the dissipation pattern in the flow.

The shape of the photospheric peak, given, for instance, by α and β of a Band function fit, can now be translated into physical properties of the dissipation, quantified by the parameters such as ϵ_e, ϵ_B and τ and dissipation rates. Depending on the details of the model we can therefore diagnose the outflow and its temporal evolution in individual bursts.

5.1 Photospheric emission

Among the main contenders for explaining the hard α values observed are (i) small-pitch-angle synchrotron emission (Epstein 1973; Epstein & Petrosian 1973) or similarly jitter radiation (Medvedev 2000, 2006) and (ii) inverse Compton emission seeded by self-absorbed synchrotron emission (Painatescu & Mészáros 2000) or by soft photons with a narrow energy distribution, i.e.

a quasi-monoenergetic distribution (Stern & Poutanen 2004). However, these non-thermal emission models typically lead to very broad spectral peaks and cannot produce spectra that are as narrow as observed (below an order of magnitude) and that are as hard ($\alpha \gtrsim 0$, see Section 2.2). For instance, inverse Compton emission leads to broad spectral peaks of typically two orders of magnitude or above (see e.g. Baring & Braby 2004; Stern & Poutanen 2004).

Moreover, studies of the acceleration processes in relativistic collisionless shocks indicate that a strong thermal component in the electron spectrum is formed (Sironi & Spitkovsky 2011). Even though the full emitting region can still not be fully simulated, these results question the classical assumption of a strong PL component of the shocked electron population. Sironi & Spitkovsky (2011) show through particle-in-cell simulations of shocks in unmagnetized pair plasmas that the width of the emitted synchrotron spectrum, in general, lies in the range of two to four orders of magnitude.

We further note that Sironi & Spitkovsky (2011) argue that if the electrons are accelerated in relativistic unmagnetized shocks then the emission is in the classical synchrotron regime rather than in the jitter radiation regime. In addition, small-pitch-angle synchrotron emission predicts a negative correlation between $E_{\rm p}$ and α, in contrast to the observed (mainly) positive correlations (Lloyd-Ronning & Petrosian 2002). These two facts pose further challenges for such an explanation for the observed hard spectra.

The narrow and hard spectra we observe in GRB090902B are thus inconsistent with the non-thermal emission models.

The photospheric model can easily overcome many of the challenges of the standard, internal-shock synchrotron model (see e.g. discussion in Ryde & Pe'er 2009). Most importantly, the (reprocessed) Planck function naturally provides very hard spectral slopes ($\alpha \leq 1$). Moreover, a PL distribution of electrons is not required to be produced by the acceleration processes; the PL slope in the BB+pl model has a preferred value of $\alpha \sim -1.5$ (Ryde et al. 2006; Ryde & Pe'er 2009). This is naturally expected due to the cooling of the electrons, which produces a PL distribution below the characteristic synchrotron frequency (the case is similar for Synchrotron Self Compton (SSC)).

An inevitable and characteristic signature of emission from the photosphere is a cut-off at energies $0.5\,\Gamma$ MeV $\gtrsim 100$ MeV due to pair production. The observation of an extension of a Band function to energies above several GeV in bursts (e.g. GRB080916c; Abdo et al. 2009a) may thus pose a challenge for (reprocessed) photospheric emission to explain the spectra. In order to overcome this difficulty, the existence of very high energy photons in the observed spectra therefore requires an additional emission site, which is capable of producing optically thin emission. We note that such a scenario (spectra indicating two emission components) is clearly observed in several bursts observed by the *Fermi*-LAT. Moreover, in one of the analysed time bins in GRB080916c there is indeed an indication of an extra PL component, even though the overall conclusion of the analysis is that a single component sufficiently fits that data (Abdo et al. 2009a). This suggests the possibility that an extra component could indeed be present in the data. However, the combined spectrum can still be satisfactorily fitted by an extension of a single Band function found at lower energies. Ghisellini et al. (2010) indeed find that the PL slope fitted to the spectrum at energies $\lesssim 40$ MeV (i.e. the Band β) and the PL slope fitted to the spectrum at energies at $\lesssim 100$ MeV are significantly different. This can be an additional indication that additional emission components are required at the highest energies, thereby alleviating this problem for the photospheric model.

5.2 Correlation between $E_{\rm p}$ and α

In Section 4.3, we discuss the observed correlation between $E_{\rm p}$ and α in terms of subphotospheric heating. A positive correlation between time-resolved $E_{\rm p}$ and α values for individual bursts was early identified by, for instance, Ford et al. (1995) , Crider et al. (1997) and Lloyd-Ronning & Petrosian (2002). More recently, Kaneko et al. (2006) found that this is the strongest correlation among GRB parameters. In a sample of 196 bursts, they found a strong correlation for 26 per cent; in most cases the correlation is stronger than the one in Fig. 7. The actual fraction of bursts exhibiting a strong correlation can be even higher, since measurement uncertainties in many cases may have masked the correlation.

The fact that not all bursts exhibit a strong correlation between $E_{\rm p}$ and α might also be an indication of that the observed spectral peaks are not directly related to kT. In some bursts, a weak contribution of a Planck function on top of a dominant Band spectrum can be identified (Ryde & Pe'er 2009; Guiriec et al. 2011). The power peaks are, in these cases, given by the non-thermal Band function and should thus not be identified by kT. As discussed in Section 3.2, this could be the case if the energy density of the electrons is much larger than the energy density of the thermal photons. Then the thermal component is expected to be relatively weak.

5.3 Change in the spectral shape from 'thermal' to 'non-thermal'

Other scenarios than the one described in Section 4.3 can be envisioned to describe a change from quasi-Planck spectrum to Band-type spectrum. For instance, Beloborodov (2010) calculated the full radiative transfer of the relativistic jet and showed that a perfect Planck function is obtained if and only if the flow is dominated by radiation, that is, the radiation energy density is much larger than the rest mass energy density of the plasma in the comoving frame of the flow. This is independent of subphotospheric dissipation since the photon energy totally dominates. However, there will inevitably be broadening due to geometrical effects (Pe'er & Ryde 2011), as discussed in Section 3.2. The spectral change observed between epochs 1 and 2 can then be due to a change from a radiation-dominated phase into a baryon-dominated phase, in which dissipation causes the strong deviation from the Planck function. An interesting consequence of such a scenario would be vanishing of the strong polarization expected during the photon-dominated phase.

Yet another possibility is if the variability time-scale and amplitude suddenly change. During epoch 2 the variations of the temperature can become large and be on a time-scale smaller than the integration time-scale. We would then measure spectra that are broader than a Planck spectrum due to significant variations of the spectral peak during the integration time. In such a case, the asymptotic slopes of the spectrum should still be those of a blackbody.

Finally, one may still envision that the emission in the MeV peak during epoch 1 is due to the photosphere, while during epoch 2 the emission is from a different, non-thermal, radiation process, for instance, from optically thin synchrotron emission. However, as discussed above the observed spectra during epoch 2 are still significantly inconsistent with what is expected from the fast-cooling electrons ($\alpha = -1.5$ and a much broader spectral width). Moreover, to get the synchrotron peak energy to lie in a similar energy range as the thermal peak during epoch 1 requires an unreasonable

coincidence. This is also not supported by the behaviour of the non-thermal (NT) part of the spectrum.

5.4 Comparison with pre-*Fermi* spectral analysis

Prior to the launch of *Fermi* we mainly had to rely on spectra in a narrow energy range, for instance that of *CGRO*-BATSE (∼25–1900 keV). The limited spectral widths made it difficult to unambiguously deduce the spectral behaviour of GRBs. Nevertheless, the importance of the photospheric emission was already alluded to (see e.g. the review by Ryde 2008). Using the broader energy range provided by *Fermi* this unambiguity can now be revealed. We can summarize the pre-*Fermi* results with the following three behaviours.

(i) Many bursts provided us with a clear indication of the photosphere. These include the spectra that are well described by a single Planck function (Ryde 2004) and the spectra for which a fit of the BB+pl model gives a statistically significant improvement over a fit with a Band function model (Ryde & Pe'er 2009). Such cases should be similar to GRB090902B observed by *Fermi*; the νF_ν peak is due to the Planck function and there are two distinct components.

(ii) Other bursts indicated that the power peak lay beyond the observed energy range, even though a subdominant thermal peak was identifiable. The thermal component forms a shoulder on the low-energy side of the power peak. The power peak of the spectrum is, in this interpretation, not directly due to the photospheric component, but due to a non-thermal emission. Examples of such spectra are given by PHEBUS *GRANAT* observations of GRB 900520a (Barat et al. 1998), *CGRO* BATSE/EGRET observations of GRB981021, BATSE trigger 7071 (González et al. 2009; Ryde & Pe'er 2009) and *Fermi* observations of GRB100724B (Guiriec et al. 2011), as well as *Fermi* cases like GRB 080916c (Abdo et al. 2009a), see also Batellino et al. (2007) and Ryde & Batellino (2005).

(iii) As argued in the study above, the thermal peak can be broadened due to subphotospheric heating, which creates a spectrum which is Band-like and significantly different from a Planck function. This mechanism is thus able to explain many Band-like spectra as well as the typical hard-to-soft spectral evolution. Apart from these facts, it also opens up the possibility that some spectra that were fitted in pre-*Fermi* analyses by a BB+pl model, in a narrow energy range, may have been misinterpreted. This could be the case particularly for bursts whose BB+pl spectral fits are not an improvement over a Band-only model fit. In these cases, the Planck function component of the fits still correctly captures the photospheric peak. However, the PL component instead captures the broadening of the peak (which makes it non-Planckian), instead of representing a real secondary component. If this is the case, such a BB+pl model would, of course, not be able to describe the broad-band spectrum of these bursts. Such spectra can explain the results in Ghirlanda et al. (2007) and Bellm (2010), who find that in some bursts a simple extension of the BB+pl model does not seem to fit the data at hand outside the BATSE energy range. We note that this is apart from the fact that the non-thermal component is expected to be a more complicated function than a single PL over a broader energy range.

6 CONCLUSION

The unambiguous signature of emission from the photosphere is a Planck function. However, subphotospheric dissipation can easily distort the photospheric emission into a broader spectrum, resembling a Band function.

The burst of 090902B made it possible for us to draw two important conclusions. First, the study of the behaviour of the MeV peak allows us to observationally claim that the origin of a Band function can be the same as the origin of a Planck spectrum; a Band spectrum can be interpreted as photospheric emission. Secondly, in order to explain the broader spectral shape of the photospheric emission, subphotospheric dissipation is needed. The existence of such dissipation is thus verified.

We show that a varying Lorentz factor of the outflow leads to a varying strength of subphotospheric dissipation. This, in turn, leads naturally to a correlation between the broadening of the spectrum and its peak energy. A correlation between α and $E_{\rm p}$, which is a consequence of this, is indeed commonly observed in GRBs.

Photospheric emission could thus be a ubiquitous signature of the prompt emission spectrum and play an important role in creating the diverse spectral shapes and spectral evolutions that are observed. The photospheric component can be dominant (e.g. GRB090902B) or subdominant (e.g. GRB100724B). It can be a Planck function throughout the burst (Ryde 2004) or it can broaden with time (as argued in this paper). An important consequence of this is that broad-band fitting of GRB spectra with only a Band function might be misleading.

ACKNOWLEDGMENTS

We thank Peter Mészáros for useful comments on the manuscript. FR wishes to express his gratitude to the Swedish National Space Board for financial support. EM acknowledges with thanks financial support from Carl Tryggers Stiftelse för Vetenskaplig Forskning and MA is supported by the Swedish Research Council (grant 2009-691).

The *Fermi*-LAT Collaboration acknowledges generous ongoing support from a number of agencies and institutes that have supported both the development and the operation of the LAT as well as scientific data analysis. These include the National Aeronautics and Space Administration and the Department of Energy in the United States, the Commissariat à l'Energie Atomique and the Centre National de la Recherche Scientifique/Institut National de Physique Nucléaire et de Physique des Particules in France, the Agenzia Spaziale Italiana and the Istituto Nazionale di Fisica Nucleare in Italy, the Ministry of Education, Culture, Sports, Science and Technology (MEXT), High Energy Accelerator Research Organization (KEK) and Japan Aerospace Exploration Agency (JAXA) in Japan, and the K. A. Wallenberg Foundation, the Swedish Research Council and the Swedish National Space Board in Sweden.

Additional support for science analysis during the operations phase is gratefully acknowledged from the Istituto Nazionale di Astrofisica in Italy and the Centre National d'Études Spatiales in France.

The *Fermi* GBM collaboration acknowledges support for GBM development, operations and data analysis from NASA in the US and BMWi/DLR in Germany.

REFERENCES

Abdo A. A. et al., 2009a, Sci, 323, 1688
Abdo A. A. et al., 2009b, ApJ, 706, L138
Asano K., Guiriec S., Mészáros P., 2009, ApJ, 705, 191
Band D. et al., 1993, ApJ, 413, L281

Barat C., Lestrade J. P., Dezalay J.-P., Hurley K., Sunyaev R., Terekhov O., Kuznetsov A., 1998, in Meegan C. A., Koshut T. M., Preece, R. D., eds, AIP Conf. Proc. Vol. 428, 4th Hunstville Gamma-Ray Bursts Symposium. Am. Inst. Phys., New York, p. 278
Baring M. G., Braby M. L., 2004, ApJ, 613, 460
Batellino M., Ryde F., Omodei N., Longo F., 2007, in Axelsson M., Ryde F., eds, AIP Conf. Proc. Vol. 906, Gamma-Ray Bursts: Prospects for GLAST. Am. Inst. Phys., New York, p. 28
Bellm E. C., 2010, ApJ, 714, 881
Beloborodov A. M., 2003, ApJ, 588, 931
Beloborodov A. M., 2010, MNRAS, 407, 1033
Bromberg O., Mikolitzky Z., Levinson A., 2011, ApJ, 733, 85
Cenko S. B. et al., 2010, ApJ, 711, 641
Crider A. et al., 1997, ApJ, 479, L39
Cucchiara A., Fox D. B., Tanvir N., Berger E., 2009, GRB Coordinates Network, 9873, 1
Eichler D., Levinson A., 2000, ApJ, 529, 146
Epstein R. I., 1973, ApJ, 183, 593
Epstein R. I., Petrosian V., 1973, ApJ, 183, 611
Ford L. A. et al., 1995, ApJ, 439, 307
Ghirlanda G., Celotti A., Ghisellini G., 2003, A&A, 406, 879
Ghirlanda G., Bosnjak Z., Ghisellini G., Tavecchio F., Firmani C., 2007, MNRAS, 379, 73
Ghisellini G., Celotti A., 1999, ApJ, 511, L93
Ghisellini G., Ghirlanda G., Nava L., Celotti A., 2010, MNRAS, 403, 926
Giannios D., 2006, A&A, 457, 763
Giannios D., 2008, A&A, 480, 305
Giannios D., Spruit H. C., 2005, A&A, 430, 1
Giannios D., Spruit H. C., 2007, A&A, 469, 1
González M. M. et al., 2009, ApJ, 696, 2155
Goodman J., 1986, ApJ, 308, L47
Guiriec S. et al., 2011, ApJ, 727, L33
Ioka K., 2010, Prog. Theor. Phys., 124, 667
Jones F. C., 1968, Phys. Rev. Lett., 167, 1159
Kaneko Y. et al., 2006, ApJS, 166, 298
Larsson J., Ryde F., Lundman C., McGlynn S., Larsson S., Ohno M., Yamaoka K., 2011, MNRAS, in press (doi:10.1111/j.1365-2966.2011.18582.x)
Lazzati D., Begelman M. C., 2010, ApJ, 725, 1137
Lazzati D., Morsony B. J., Begelman M. C., 2009, ApJ, 700, L47
Lloyd-Ronning N. M., Petrosian V., 2002, ApJ, 565, 182
McKinney J. C., Uzdensky D. A., 2010, preprint (arXiv:1011.1904)
Medvedev M. V., 2000, ApJ, 540, 704
Medvedev M. V., 2006, ApJ, 637, 869
Meegan C. et al., 2009, ApJ, 702, 791
Mészáros P., Rees M. J., 2000, ApJ, 530, 292
Mészarós P., Ramirez-Ruiz E., Rees M. J., Zhang B., 2002, ApJ, 578, 812
Mizuta A., Nagataki S., Aoi J., 2011, ApJ, 732, 26
Morsony B. J., Lazzati D., Begelman M. C., 2010, ApJ, 723, 267
Nagakura H., Ito H., Kiuchi K., Yamada S., 2011, ApJ, 731, 80
Paczyński B., 1986, ApJ, 308, L43
Panaitescu A., Mészáros P., 2000, ApJ, 544, L17
Pe'er A., 2008, ApJ, 682, 463
Pe'er A., Ryde F., 2011, ApJ, 732, 49
Pe'er A., Waxman E., 2004, ApJ, 613, 448
Pe'er A., Waxman E., 2005, ApJ, 628, 857
Pe'er A., Mészáros P., Rees M. J., 2005, ApJ, 635, 476
Pe'er A., Mészáros P., Rees M. J., 2006, ApJ, 642, 995
Pe'er A., Ryde F., Weijers R., Mészarós P., Rees M., 2007, ApJ, 664, L1
Pe'er A., Zhang B. B., Ryde F., McGlynn S., Zhang B., Preece R., Kouveliotou C., 2010, preprint (arXiv:1007.2228)
Pe'er A., Zhang B.-B., Ryde F., McGlynn S., Zhang B., Preece R. D., Kouveliotou C., 2011, preprint (arXiv:1007.2228)
Preece R. D., Briggs M., Malozzi R., Pendleton G., Paciesas W. S., Band D. L., 1998, ApJ, 506, 23
Preece R. D., Briggs M., Giblin T., Malozzi R., Pendleton G., Paciesas W., Band D., 2002, ApJ, 581, 1248
Ramirez-Ruiz E., 2005, MNRAS, 363, L61
Razzaque S., Dermer C. D., Finke J. D., 2010, Open Astron. J., 3, 150
Rees M. J., Mészáros P., 1994, ApJ, 430, L93
Rees M. J., Mészáros P., 2005, ApJ, 628, 847
Ruffini R., Bianco C. L., Xue S.-S., Chardonnet P., Fraschetti F., Gurzadyan V., 2005, Int. J. Modern Phys. D, 14, 97
Rybicki G. B., Lightman A., 1979, Radiative Processes in Astrophysics. Wiley, New York
Ryde F., 2004, ApJ, 614, 827
Ryde F., 2005, ApJ, 625, L95
Ryde F., 2008, Phil. Trans. R. Soc. A, 366, 4405
Ryde F., Batellino M., 2005, Nuovo Cimento C Geophysics Space Phys. C, 28, 335
Ryde F., Pe'er A., 2009, ApJ, 702, 1211
Ryde F. et al., 2006, ApJ, 652, 1400
Ryde F. et al., 2010, ApJ, 709, L172
Sironi L., Spitkovsky A., 2011, ApJ, 726, 75
Stern B., Poutanen J., 2004, MNRAS, 352, L35
Tavani M., 1996, ApJ, 466, 768
Tchekhovskoy A., McKinney J. C., Narayan R., 2008, MNRAS, 388, 551
Thompson C., 1994, MNRAS, 270, 480
Toma K., Wu X.-F., Mészáros P., 2010, preprint (arXiv:1002.2634)
Zhang W., Woosley S. E., Heger A., 2004, ApJ, 608, 365
Zhang B.-B. et al., 2011, ApJ, 730, 141

This paper has been typeset from a TEX/LATEX file prepared by the author.